

STRUCTURAL AND OPTICAL STUDY OF COPPER DOPED ZINC SULFIDE NANOPARTICLES****P. Mishra¹, K. S. Ojha^{2*}, A. Khare²**¹ Parala Maharaja Engineering College, Brahmapur, Odisha-761003, India² National Institute of Technology Raipur-492010, India; e-mail: kspectra12@yahoo.co.in

Copper doped zinc sulfide nanoparticles have been synthesized using a wet chemical method. The synthesized nanoparticles exhibit a zinc blende structure with the crystallite size of 3.8 nm. The morphological and optical studies of the synthesized nanoparticles have been performed. It is found that the band gap varies from 3.6 to 4.4 eV depending upon the concentration of copper. The room temperature photoluminescence of the synthesized nanoparticles has been also investigated.

Keywords: ZnS, ZnS:Cu, X-ray diffractometry, scanning electron microscopy, transmission electron microscopy, nanoparticles, photoluminescence.

ИССЛЕДОВАНИЕ СТРУКТУРЫ И ОПТИЧЕСКИХ ХАРАКТЕРИСТИК НАНОЧАСТИЦ ЛЕГИРОВАННОГО МЕДЬЮ СУЛЬФИДА ЦИНКА**P. Mishra¹, K. S. Ojha^{2*}, A. Khare²**

УДК 535.37;620.3

¹ Технический колледж Парала Махараджа, Брамапур, Одисша, 761003, Индия² Национальный технологический институт, Райпур, 492010, Индия; e-mail: kspectra12@yahoo.co.in

(Поступила 18 апреля 2017)

Методом мокрой химии синтезированы наночастицы сульфида цинка, легированного медью. Полученные частицы обладают кристаллической структурой цинковой обманки с размером кристаллита 3.8 нм. Исследованы морфологии и оптические характеристики синтезированных частиц. Обнаружено, что ширина запрещенной зоны изменяется от 3.6 до 4.4 эВ в зависимости от концентрации меди. Исследована фотолюминесценция частиц при комнатной температуре.

Ключевые слова: ZnS, ZnS:Cu, рентгеноструктурный анализ, сканирующая электронная микроскопия, просвечивающая электронная микроскопия, наночастица, фотолюминесценция.

Introduction. Recently, metal-doped II-VI semiconductors have attracted much attention due to their self-assembled different types of nanostructures. The doped metals make these semiconductors more energetic and attractive [1], and such materials exhibit luminescence properties due to the presence of impurity ions [1–5]. Different types of dopants and their concentrations are responsible for the luminescence band position, as well as efficiency of the materials. Zinc sulfide, synthesized in various forms, demonstrates diverse applications as optical devices [6–15]. The luminescence properties of metal-doped ZnS nanostructure have been studied by several workers. An intra-ionic transition between $^4f_7-^4f_6^5d_1$ states of Eu^{2+} ions has been reported in ZnS:Eu nanoparticles (NPs) [16, 17]. Similarly, an orange emission band due to the transition between $^4T_1-^6A_1$ states of Mn^{2+} ions has been observed in ZnS:Mn NPs [18–20]. ZnS:Cu NPs, one of the important luminescent materials, have been synthesized and characterized by several workers along with the material luminescence properties [21–25]. Two luminescence bands of ZnS:Cu NPs close to 420 and 520 nm have been reported Lee et. al. [22], while Xu et al. [17] observed two luminescence bands close to

** Full text is published in JAS V. 85, No. 4 (<http://springer.com/10812>) and in electronic version of ZhPS V. 85, No. 4 (http://www.elibrary.ru/title_about.asp?id=7318; sales@elibrary.ru).

460 and 507 nm. Luminescence peaks close to 480 and 415 nm have been observed by Kulkarni et al. [21] and Shen et al. [23], respectively, while a peak close to 600 nm due to the transition between trapped electron and Cu^{2+} ions has been observed by Bol et al. [24]. Recently, Wang et al. [26] observed three luminescence bands (two in a blue region and one in a green region) and reported that the green peak shifted towards longer wavelength is due to an increase in Cu^{2+} ion concentration. A mixed type structure containing both cubic zinc blende and wurtzite hexagonal phases along with enhanced bandgap energy has been observed in ZnS:Cu NPs by Kalita et al. [27]. A tunable emission ranging from blue to red regions has been observed by Golberg et al. [28] in ZnS and Mn/Cu-doped ZnS NPs, and it has been also reported that such emission is powerful and steady. From the above literature, it is seen that there is still controversy the luminescence properties of ZnS:Cu NPs. Therefore, it is decided to synthesize the ZnS:Cu nanoparticles using a wet chemical route and explore the luminescence properties of ZnS:Cu NPs.

Materials and methods. ZnS:Cu NPs have been synthesized via the method described by Manuspiy et al. [29]. Raw materials of zinc sulfate, sodium sulfide, and cuprous chloride, all of purity 99.99%, along with distilled water and methanol (analytical grade), are used to synthesize ZnS:Cu NPs. Two separate mixtures, one of $\text{Na}_2\text{S} \cdot 9\text{H}_2\text{O}$ and distilled water and the other of $\text{ZnSO}_4 \cdot 7\text{H}_2\text{O}$ with distilled water, are prepared, and each prepared mixture is stirred for 1 h. After complete stirring, both solutions are mixed together to prepare ZnS NPs. Two separate mixtures, one of $\text{Na}_2\text{S} \cdot 9\text{H}_2\text{O}$ with distilled water and the other of $\text{ZnSO}_4 \cdot 7\text{H}_2\text{O}$, the appropriate amount of CuCl, and distilled water are used to prepare ZnS:Cu NPs. Each mixture is separately stirred for 1 h and then mixed into each other. To complete the reaction, the mixture is kept for 4 h at room temperature. Methanol is used to remove the impurities. After removing the impurities, the mixture is centrifuged at 1000 rpm for 20 min, and then the prepared samples are washed with deionized water and methanol. The synthesized NPs with different copper concentrations are dried under vacuum for characterization.

Analysis and result. *Structural study.* A X-ray diffractometer (Rigaku-Miniflex) with $\text{CuK}\alpha$ line ($\lambda = 1.5406 \text{ \AA}$) is used to study the structure and phase of pure ZnS and ZnS:Cu NPs. The XRD patterns, consisting of three distinct peaks of the synthesized samples, are shown in Fig. 1. The observed peaks correspond to (111), (220), and (311) planes of the cubic zinc blende structure and confirm the purity of the synthesized NPs. The peak corresponding to (111) shows broadening as well as less relative intensity with increasing copper concentration. The broadening observed in (111) peak indicates the degradation of crystallite size due to doping of copper, as well as the nanocrystalline nature of ZnS [24] of the sample from the XRD patterns. The crystallite size, calculated using Scherrer's formula, is found to be 5–3.7 nm for pure and ZnS:Cu NPs. The crystallite size of pure ZnS NPs is about 5 nm; but with increasing doping concentration, the crystallite size decreases from 5.0 to 3.7 nm. The major change in the crystallite size is observed at 1.0 mol.% Cu doping, but after increasing the Cu concentration, slight changes are observed in the crystallite size, as shown in Table 1.

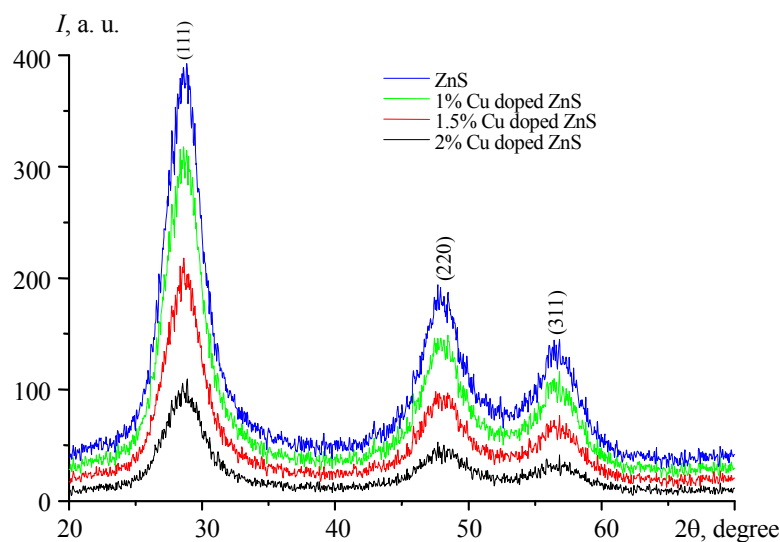


Fig. 1. X-ray diffraction pattern of pure and ZnS:Cu nanoparticles.

TABLE 1. Crystallite Size of Pure and ZnS:Cu Nanoparticles

β (FWHM)				Crystallite size D (nm) from XRD			
0	1	1.5	2.0	0	1	1.5	2.0
3.1	3.9	4.1	4.3	5.1	4.1	3.75	3.65

Note. $(hkl) = (111)$, $2\theta = 28.62^\circ$.

Surface morphology. The surface morphology of pure and ZnS:Cu NPs has been studied using scanning electron microscope (SEM, ZESIS) operating at 15 kV. The SEM micrograph, represented in Fig. 2, confirms the spherical shape with the average size of 5 nm for undoped ZnS. The average particle size decreases from 5 to 3.7 nm with increase in copper concentration from 0.0 to 1.0 mol.% and becomes almost constant for 1.5 and 2.0 mol.% of Cu concentration [1]. The average particle size of ZnS:Cu NPs has also been estimated using transmission electron microscope (TEM) operating at 200 kV and is found to be 3.5 nm, which is in close agreement with that observed from XRD and SEM. A TEM image of ZnS:Cu NPs for 1.5 mol.% of Cu concentration is shown in Fig. 2e.

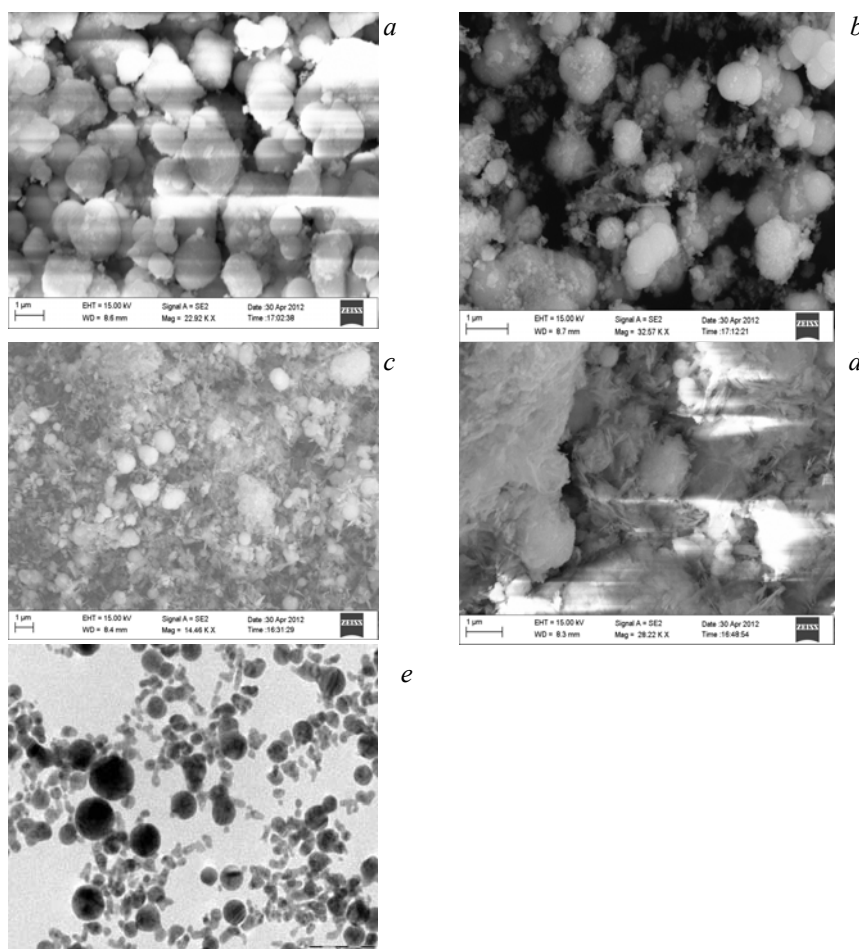


Fig. 2. SEM micrographs of pure ZnS (a), ZnS:Cu nanoparticles (b–d), and TEM image of 1.5 % Cu doped ZnS nanoparticles (e).

Optical study. The optical characteristics of the synthesized samples has been investigated using an UV-Vis spectrophotometer (Perkin Elmer, USA). The UV-visible absorption spectra and a tauc plot of pure and ZnS:Cu NPs are shown in Fig. 3. A hump close to 318 nm is observed in ZnS:Cu NPs and is shifted toward the red end of the spectrum with increasing concentration of copper. The calculated energy gap of ZnS:Cu NPs is found to be 3.92 eV, which is large in comparison with the pure ZnS (~3.6 eV), and this enhancement is attributed to the quantum confinement effect.

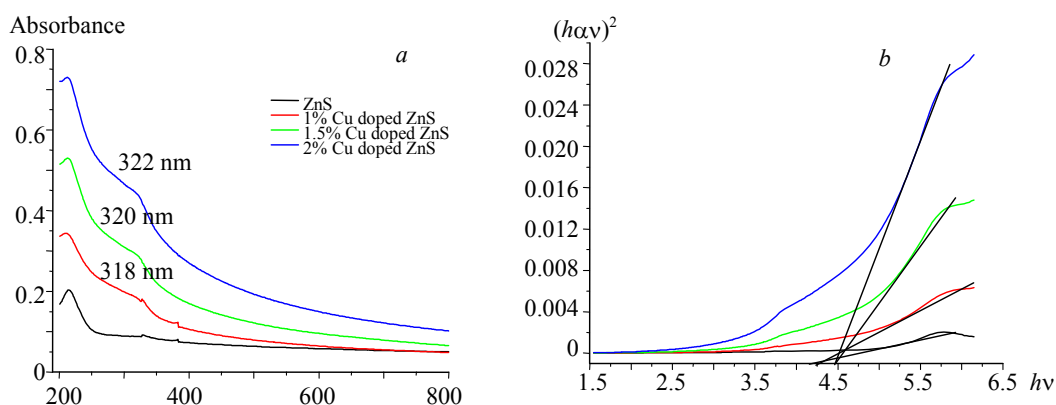


Fig. 3. Uv-Vis absorption spectra (a) and Tauc plot of pure and ZnS:Cu nanoparticles (b).

Photoluminescence study. The room temperature PL spectra of the synthesized NPs are recorded using a fluorescence spectrophotometer (Jobin Yvon, USA). The observed spectra are broad and asymmetric, therefore deconvoluted, and are represented in Fig. 4. The positions of the luminescence bands are shown in Table 2. Two luminescence bands lying at 410 and 450 nm are observed in pure ZnS NPs, while in the case of ZnS:Cu NPs, along with these two bands, a third band lying at 490 nm has also been observed. The band lying at 410 nm is from the transition between the donor level of the sulfur vacancy. The valence band [8] and its position are almost constant for pure, 1 and 2 mol.% ZnS:Cu NPs, but for 1.5 mol.% ZnS:Cu NPs, there is a slight red shift in the position, which may be due to agglomeration of NPs. The peak lying at 450 nm is attributed to the emission between the zinc sulfide conduction band and Cu^{2+} ion energy level (t_2 level) [9], while the transition of trap states of ZnS is responsible for a similar peak observed in the case of pure ZnS NPs [15, 16]. The position of this peak is almost independent of Cu^{2+} ions concentration and confirms that defect states of zinc are responsible for this band. The intensity of the peak centered at 450 nm for ZnS NPs is much smaller than that of the doped samples (Fig. 4).

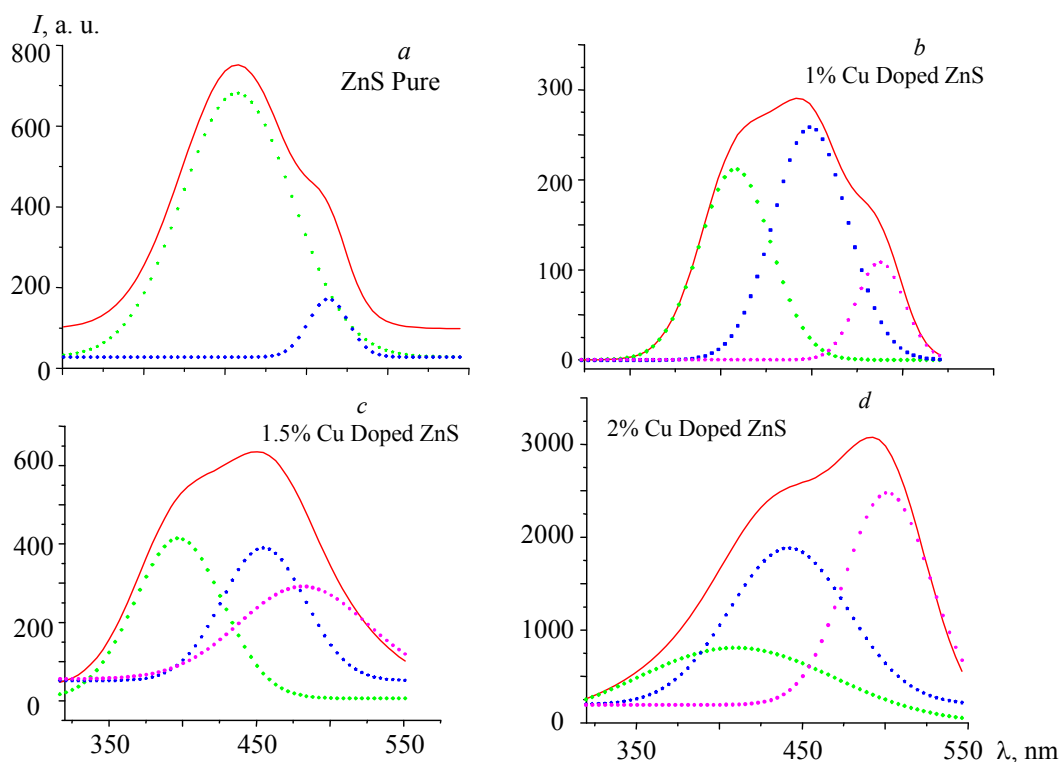


Fig. 4. Photoluminescence spectra of pure and ZnS:Cu nanoparticles.

This can be explained on the basis of the doping effect according to which Cu^{2+} ions doped into ZnS NPs introduce more defects. But, for the peak centered at 411 nm, the reverse effect has been observed in this study, which may be due to agglomeration of NPs. In the case of the ZnS:Cu nanostructure, the band observed at 490 nm is in agreement with the earlier report [9] and results from the transition between the sulfur vacancy donor level and Cu^{2+} ions (t_2 level). The position of this band shifts toward the red end (from 490 to 500 nm) as the concentration of Cu^{2+} ion increases. The energy difference between the sulfur-related vacancy level and the zinc sulfide conduction band is almost constant with variation in copper concentration. This confirms that the energy difference between the Cu^{2+} ions level (t_2) and the valence band of zinc sulfide is very large.

TABLE 2. Photoluminescence Peak Positions (nm) of Pure and ZnS:Cu Nanoparticles

C_{Cu} , mol.%	Peak I	Peak II	Peak III
0.0	409.1	454.2	–
1.0	410.8	449.3	490.3
1.5	403.6	454.3	490.8
2.0	411.8	447.4	500.9

Conclusion. ZnS:Cu nanoparticles of about 3.7 nm size have been synthesized using a wet chemical route. The XRD pattern exhibits the zinc blende structure, and SEM confirms its spherical shape. The PL spectra of the pure ZnS nanoparticles show two blue luminescence bands, while those of the ZnS:Cu nanoparticles shows a third peak in the green region along with the two blue bands. The band lying in the green region is due to copper, while zinc sulfide defect states are responsible for the blue bands. In photoluminescence, the relaxation of photo-excited conduction electrons of ZnS to certain surface states of Cu^{2+} ions takes place, and a radiative transition occurs that generates luminescence in the visible region. The doping of Cu^{2+} ions into the host ZnS nanoparticles enhances the photoluminescence quantum efficiency of the host due to the strong interaction between electrons and holes with localized states of Cu^{2+} ions. The enhanced luminescent properties of the ZnS:Cu nanoparticles makes them potential candidates for applications in optical sensors, light emitting diodes, flat panel displays, lasers, and light emitting displays.

REFERENCES

1. M. Wang, L. Sun, X. Fu, C. Liao, C. Yan, *Solid State Commun.*, **115**, 493–496 (2000).
2. H. Y. Lu, S. Y. Chu, *J. Cryst. Growth*, **265**, 476–481 (2004).
3. D. Denzler, M. Olschewski, K. Sattler, *J. App. Phys.*, **84**, 2841–2845 (1998).
4. P. Yang, M. Lu, D. Xu, D. Yuan, G. Zhou, *Chem. Phys. Lett.*, **336**, 76–80 (2001).
5. K. Jayanthi, S. Chawla, H. Chander, D. Haranath, *Cryst. Res. Technol.*, **42**, 976–982 (2007).
6. J. M. Hwang, M. O. Oh, I. Kim, J. K. Lee, C. S. Ha, *Curr. Appl. Phys.*, **5**, 31–34 (2005).
7. H. Cho, C. Yun, J. W. Park, S. Yoo, *Org. Electron.*, **10**, 1163–1169 (2009).
8. C. W. Lee, C. H. Chou, J. H. Huang, C. S. Hsu, T. P. Nguyen, *Mater. Sci. Eng. B*, **147**, 307–311(2008).
9. X. Liu, X. Cai, J. Mao, C. Jin, *Appl. Surf. Sci.*, **183**, 103–110 (2001).
10. V. Dimitrova, J. Tate, *Thin Solid Films*, **365**, 134–138 (2000).
11. D. W. Wang, S. L. Zhao, Z. Xu, C. Kong, W. Gong, *Org. Electron.*, **12**, 92–97 (2011).
12. E. A. Mastio, C. B. Thomas, W. M. Cranton, E. Fogarassy, *Appl. Surf. Sci.*, **157**, 74–80 (2000).
13. B. L. Zhu, X. Chen, L. M. Xu, *Thin Solid Films*, **474**, 114–118 (2005).
14. C. Ma, D. Moore, J. Li, Z. L. Wang, *Adv. Mater.*, **15**, 228–231 (2003).
15. Y. Zhao, Y. Zhang, H. Zhu, G. C. Hadjipanayis, J. Q. Xiao, *J. Am. Ceram. Soc.*, **126**, 6874–6875 (2004).
16. W. Chen, J. O. Malm, V. Zwiller, Y. Huang, S. Liu, R. Wallenberg, J. O. Bovin, L. Samuelson, *Phys. Rev. B*, **61**, 11021–11024 (2000).
17. S. J. Xu, S. J. Chua, B. Liu, L. M. Gan, C. H. Chew, G. Q. Xu, *Appl. Phys. Lett.*, **73**, 478–480 (1998).
18. B. Y. Geng, L. D. Zhang, G. Z. Wang, T. Xie, Y. G. Zhang, G. W. Meng, *Appl. Phys. Lett.*, **84**, 2157–2159 (2004).
19. B. Bhattacharjee, D. Ganguli, K. Iakoubovskii, A. Stesmans, S. Chaudhuri, *Bull. Mater. Sci.*, **25**, 175–180 (2002).
20. R. N. Bhargava, D. Gallagher, X. Hong, A. Nurmikko, *Phys. Rev. Lett.*, **72**, 416–419 (1994).

21. A. A. Khosravi, M. Kundu, L. Jatwa, S. K. Deshpande, U. A. Bhagwat, M. Sastry, S. K. Kulkarni, *Appl. Phys. Lett.*, **67**, 2702–2704 (1995).
22. S. Lee, D. Song, D. Kim, J. Lee, S. Kim, I. Y. Park, and Y. D. Choi, *Mater. Lett.*, **58**, 342–346 (2004).
23. J. Huang, Y. Yang, S. Xue, B. Yang, S. Liu, J. Shen, *Appl. Phys. Lett.*, **70**, 2335–2337 (1997).
24. A. A. Bol, J. Ferwerda, J. A. Bergwer, A. Meijerink, *J. Lumin.*, **99**, 325–334 (2002).
25. S. Lee, D. Song, J. Lee, S. Kim, I. Y. Park, M. S. Won, *Mater. Sci. Eng. B*, **103**, 241–245 (2003).
26. W. Q. Peng, G. W. Cong, S. C. Qu, Z. G. Wang, *Opt. Mater.*, **29**, 313–317 (2006).
27. B. Bodo, P. K. Kalita, *Res. J. Phys. Sci.*, **1**, 2–5 (2013).
28. B. Liu, Y. Bando, X. Jiang, C. Li, X. Fang, H. Zeng, T. Terao, C. Tang, M. Mitome, D. Golberg, *Nanotechnology*, **21**, 375601 (2010).
29. S. Ummartyotin, N. Bunnak, J. Juntaro, M. Sain, H. Manuspiya, *Solid State Sci.*, **14**, 299–304 (2012).